AIP Advances

3D engineered neural co-culture model and neurovascular effects of marine fungi-derived citreohybridonol

Cite as: AIP Advances **12**, 095102 (2022); https://doi.org/10.1063/5.0100452
Submitted: 01 June 2022 • Accepted: 06 August 2022 • Published Online: 07 September 2022

Emel Sokullu, İrem Polat, Ferhat Can Özkaya, et al.

View Online Export Citation CrossMark

ARTICLES YOU MAY BE INTERESTED IN

A review of marine controlled-source electromagnetic data preprocessing technology
AIP Advances **12**, 090701 (2022); https://doi.org/10.1063/5.0090082

Modeling of processing parameters for the cutting of rolled tungsten plates via abrasive water jet
AIP Advances **12**, 095103 (2022); https://doi.org/10.1063/5.0114050

An Au_{25}-R single-molecule tidal diode induced by the asymmetrical coupling
AIP Advances **12**, 095104 (2022); https://doi.org/10.1063/5.0110804



AIP Publishing

© 2022 Author(s).

3D engineered neural co-culture model and neurovascular effects of marine fungi-derived citreohybridonol

Cite as: AIP Advances 12, 095102 (2022); doi: 10.1063/5.0100452
Submitted: 1 June 2022 • Accepted: 6 August 2022 •
Published Online: 7 September 2022

View Online Export Citation CrossMark

Emel Sokullu,[1,a)] İrem Polat,[2] Ferhat Can Özkaya,[3] Mona El-Neketi,[4] Weaam Ebrahim,[4] Misagh Rezapour Sarabi,[5] Gulgun Sengul,[6] and Savas Tasoglu[5,7,8,9,10,a)]

AFFILIATIONS

[1]School of Medicine, Department of Biophysics, KUTTAM, Koc University, 34450 Istanbul, Turkey
[2]Graduate School of Nanoscience and Nanotechnology, Department of Natural and Applied Sciences, Izmir Katip Celebi University, 35620 Izmir, Turkey
[3]EBILTEM, Ege University Science and Technology Centre, 35100 İzmir, Turkey
[4]Department of Pharmacognosy, Faculty of Pharmacy, Mansoura University, 35516 Mansoura, Egypt
[5]Department of Mechanical Engineering, Koc University, 34450 Istanbul, Turkey
[6]Anatomy Department, School of Medicine, Ege University, 35040 Izmir, Turkey
[7]Koc University Arcelik Research Center for Creative Industries (KUAR), Koc University, 34450 Istanbul, Turkey
[8]Koc University Is Bank Artificial Intelligence Lab (KUIS AI Lab), Koc University, 34450 Istanbul, Turkey
[9]Bogazici Institute of Biomedical Engineering, Bogazici University, 34684 Istanbul, Turkey
[10]Koc University Translational Medicine Research Center (KUTTAM), Koc University, 34450 Istanbul, Turkey

[a)]**Authors to whom correspondence should be addressed:** esokullu@ku.edu.tr and stasoglu@ku.edu.tr

ABSTRACT

Marine-based biomolecules are emerging metabolites that have gained attention for developing novel biomaterials, drugs, and pharmaceutical *in vitro* platforms. Here, we developed a 3D engineered neural co-culture model via a 3D prototyped sliding frame-platform for multi-step UV lithography and investigated the neurovascular potential of citreohybridonol in neuroblastoma treatment. Citreohybridonol was isolated from a sponge-derived fungus *Penicillium atrovenetum*. The model was characterized by Fourier-transform infrared spectroscopy and scanning electron microscopy analysis. Human umbilical cord vein endothelial cells (HUVECs) and neuroblastoma (SH-SY5Y) cell lines were encapsulated in gelatin methacrylate (GelMA) with and without citreohybridonol. The effect of citreohybridonol on the proliferation capacity of cells was assessed via cell viability and immunostaining assays. GelMA and 3D culture characterization indicated that the cells were successfully encapsulated as axenic and mixed with/without citreohybridonol. The cytotoxic test confirmed that the 3D microenvironment was non-toxic for cultural experiments, and it showed the inhibitory effects of citreohybridonol on SH-SY5Y cells and induced the proliferation of HUVECs. Finally, immunohistochemical staining demonstrated that citreohybridonol suppressed SH-SY5Y cells and induced vascularization of HUVECs in mixed 3D cell culture.

© 2022 Author(s). All article content, except where otherwise noted, is licensed under a Creative Commons Attribution (CC BY) license (http://creativecommons.org/licenses/by/4.0/). https://doi.org/10.1063/5.0100452

I. INTRODUCTION

Neuroblastoma is an extracranial neoplasm of the autonomic nervous system and has been touted as the most common and malignant solid tumor of childhood and infancy.[1] Moreover, neuroblastoma has one of the highest mortality and morbidity rates among children.[2] Angiogenesis, known as a permanent biological process that plays an important role in the progression of neoplastic tissues in the tumor microenvironment, is a fundamental factor responsible for metastatic spread of tumors.[3] During

© Author(s) 2022

angiogenesis, new capillaries are germinated from existing vessels, leading to the development of a vascular network, which enables the growth and spread of neoplastic mass (metastatic tumors) indefinitely.[4] Angiogenesis of tumors mostly depends on the secretion of different growth factors, such as the vascular endothelial growth factor (VEGF), the fibroblast growth factor (FGF), tumor necrosis factor-alpha (TNF-α), transforming growth factor-beta (TGF-β), and angiopoietins (Ang), to stimulate pre-existing endothelial cells in a vascular bed, which subsequently leads to the growth of blood vessels in the tumor microenvironment.[4,5] Therefore, the inhibition of angiogenesis can be considered as a promising approach for cancer treatment. Most inhibitor molecules, such as statins, including endostatin, tumstatin, and angiostatin, are derived from large molecules and are not considered as functional angiogenic inhibitors.[6] Thus, the need for new agents that can inhibit vascularization and stop the spreading of metastatic cells is an increasing demand for the treatment of neuroblastoma in children.

A prerequisite for formulating a treatment procedure is an appropriate pre-translation practice such as engineering human tissue modeling, investigating on animal models, or performing *in vitro* disease modeling experiments.[7,8] Modeling human organ or tissue environments with analysis of application of the proposed treatment on that particular microenvironment is a convenient path in this regard, being usually cost-efficient with no need for ethical approval. When cells were cultured in 2D monolayers, they displayed significant differences in gene expression compared to cells in native tissues and under 3D culture conditions.[9] Since human tissues consist of 3D extracellular matrix components with several cell types, 3D models have gained more attention than 2D models since they offer more similarity and better accuracy.[10–14] On the other hand, 2D models are not usually capable enough to investigate the physiological and pathological processes of the tissues and do not effectively represent the complex 3D tissue environment.[15] 3D-engineered *in vitro* cell culture models, in contrast, present useful information about morphology, cell–cell and cell–matrix interactions, and cell differentiation.[16–19] In addition, 3D *in vitro* models are also beneficial in investigation of regeneration in tissues and organs after cancer treatment or organ loss.[20–22] In this context, utilization of various types of natural and synthetic polymers in tissue engineering methods has been demonstrated successfully in pre-clinical settings. Biocompatible and bio-inert polymers are appropriate platforms based on the release pattern of sustained bioactive molecules.[23] In particular, hydrogels such as hyaluronic acid, chitosan, the hyaluronan methylcellulose (HAMC) blend, and agarose exhibit suitable mechanical properties that qualify them for transplanting and maintaining mechanical homogeneity of the target site by cooperation of the surrounding tissues.[24–26] Furthermore, polymers, especially hydrogels, can be utilized for delivery of therapeutic molecules.[10–14] However, establishment of a desirable porous structure is not always straightforward. Polylactic acid (PLA), polyglycolic acid (PGA), polycaprolactone (PCL), chitosan, gelatin, and gelatin methacrylate (GelMA), due to their porous structures, have been used for scaffold construction in 3D cell culture systems. GelMA, an engineered gelatin-based hydrogel, offers several advantageous features, such as biocompatibility, enzymatic cleavage, proper adhesion to cells, degradation in response to matrix metalloproteinases, and controllable mechanical properties, that turn it into an outstanding versatile option for tissue engineering, drug delivery, and 3D printing applications.[27–29]

3D cell culture systems can be used not only to elucidate the cell proliferation, differentiation, and identification of growth factors but also to understand the related downstream pathways of different cell types under pathological and physiological conditions and to determine the effects of drug-candidate molecules on cell–cell and cell–matrix interactions in the disease models.[10,30–33] Co-cultivation of two or more different cell types can lead to identification of the cell-interaction effects on tissue formation by mimicking the natural environment in a laboratory.[29] For example, native tissue compartments have been mimicked via 3D co-culture protocols to observe the ecological behavior of cell populations and the effect of extracellular environment on synthetic biology and tissue regeneration.[34,35] Furthermore, 3D co-culture systems are commonly used for the investigation of the effect of chemotherapeutic drugs on tumor cells.[11] Thus, 3D *in vitro* co-culture can offer solutions to the challenges of the low success rate of clinical trials and the expensive and time-consuming processes of drug discovery.[36–39] Besides, the real potential of the drug can be identified at the beginning of the investigations.

Due to their chemical and bioactivity diversity, marine natural products such as sponge-associated fungi have been spotlighted for tolerating extreme physicochemical living conditions such as low temperature level, high salinity, and utmost living competition.[40,41] Besides, having a bigger genome size than other micro-organisms (e.g., bacteria and microalgae) makes sponge-associated fungal strains one of the most promising sustainable sources for drugs and drug-lead-compounds.[42] Here, our goal is to investigate the neurovascular effectiveness of meroterpenoid citreohybridonol, isolated from a sponge-derived fungus *Penicillium atrovenetum*. We developed a 3D engineered neural model via construction of a 3D micro-frame co-cultural microenvironment for multi-step UV lithography. Human umbilical cord vein endothelial cells (HUVECs) and neuroblastoma (SH-SY5Y) cell lines were utilized in the proposed platform. Characterization of the model was carried out using Fourier-transform infrared spectroscopy (FTIR) and scanning electron microscopy (SEM) analysis. HUVEC and SH-SY5Y cell lines were encapsulated inside a GelMA hydrogel with and without citreohybridonol. The effect of citreohybridonol on the proliferation capacity of cells was assessed via cell viability and immunostaining assays. GelMA and 3D culture characterization indicated that cells were successfully encapsulated as axenic and mixed with/without citreohybridonol. In order to evaluate the toxicity of the 3D microenvironment, cytotoxic test was performed, demonstrating non-toxicity for cultural experiments. Immunohistochemical staining also expressed that citreohybridonol suppressed SH-SY5Y cells and induced vascularization of HUVECs in the mixed 3D cell culture. Our study showed successful isolation of citreohybridonol from the sponge-associated fungus *Penicillium atrovenetum*, construction of a 3D microenvironment, and neurovascular efficiency of citreohybridonol on cancerous tissues via engineered tissues in a 3D microenvironment, resulting in a hallmark in neurovascular research.

© Author(s) 2022

II. MATERIALS AND METHODS

A. Isolation of citreohybridonol

The sponge *Spirastrella cunctatrix*-associated fungus *Penicillium atrovenetum* was cultivated on a 1 L Erlenmeyer flask containing a solid rice medium (100 g rice, 3.5 g artificial sea salt, and 110 ml distilled water) for 4 weeks under static conditions on a stationary bench and at room temperature (20–25 °C). The culture was then extracted with ethyl acetate, EtOAc (4 × 350 ml), and 4.5 g of the crude extract was obtained. This crude extract was partitioned between 90% solution of MeOH in water and *n*-hexane to yield 2 g of hydromethanolic extract. The 2 g fraction was subjected to a Sephadex LH-20 column and eluated with DCM:MeOH (1:1) to yield 10 subfractions. Fr 8 (750 mg) was fractioned via a Sephadex LH-20 column and eluated with acetone. Finally, subfraction Fr 8.1 was crystallized in MeOH to obtain anti-neuroinflammatory meroterpenoid citreohybridonol (supplementary material Fig. 1) (13 mg).[43–45]

Citreohybridonol, white powder; UV spectrum: λ_{max} (MeOH): 260, 320, 356, and 390 nm: $[\alpha]_D$:[20] +32 (c = 0.07, $CHCl_3$): HRESIMS $[M+H]^+$ m/z 501.2480 (calculated for $C_{28}H_{37}O_8$, 501.2483). ^{1}H NMR (600 MHz, DMSO-d_6, δ, ppm, *J*/Hz): 2.02 (m, H_2-1a), 1.20 (m, H_2-1b), 1.61 (m, H_2-2a), 1.54 (m, H_2-2b), 4.51 (m, H-3), 1.84 (m, H-5), 4.89 (d, 3.7, H-6), 3.05 (m, H-7a), 2.34 (m, H-7b), 2.26 (m, H-9), 5.54 (m, H-11), 1.58 (s, H_3-18), 1.15 (s, H_3-20), 1.76 (s, H_3-21), 1.22 (s, H_3-22), 0.90 (s, H_3-24), 0.79 (s, H_3-25), 2.00 (s, H_3-27), 3.55 (s, H_3-28): ^{13}C NMR (150 MHz, DMSO-d_6, δ, ppm) 20.6 (C-1), 21.5 (C-2), 75.2 (C-3), 33.9 (C-4), 54.3 (C-5), 76.9 (C-6), 37.0 (C-7), 40.9 (C-8), 51.1 (C-9), 43.0 (C-10), 121.9 (C-11), (C-12, not detected), 121.9 (C-13, not detected), 68.5 (C-14), 179.4 (C-15), 114.7 (C-16), 198.3 (C-17), 6.5 (C-18), 170.2 (C-19), 17.1 (C-20), 19.8 (C-21), 23.6 (C-22), 178.5 (C-23), 25.8 (C-24), 21.7 (C-25), 169.6 (C-26), 20.7 (C-27), 51.7 (C-28).

B. Construction of stainless-steel blocks and surface treatment

Initially, the stainless-steel solid blocks and the 3D microframe were designed with SolidWorks CAD software (ordered from YÖNSİS, Izmir, Türkiye) [supplementary material Fig. 2(a)]. These blocks were fastened by screws [supplementary material Fig. 2(b)] for preparing sensitive and stable hydrogel blocks. The black frame was designed to be 22 × 22 mm^2, and the photomasks were of the size 12 ×12 mm^2 in the black frame. The photomasks were formed by squares with a size of 300 × 300, 100, and 500 μm [supplementary material Fig. 2(c)]. Donut photomasks were constructed in a size of 1000 and 500 μm [supplementary material Fig. 2(d)]. These blocks were put in the 10% sodium hydroxide solution for one hour to improve the adhesive property of their surfaces. Then, they were washed with distilled water three times and dried in an 80 °C oven.

The surfaces of stainless blocks were covered with 3-(trimeth oxysilyl) propyl methacrylate (TMSPMA) (Sigma-Aldrich, St. Louis, MO, USA) to obtain a three-dimensional macro-porous scaffold. The blocks were incubated at 80 °C for 24 h in the TMSPMA solution. The solution was removed, and the blocks were rinsed with ethanol to eliminate the unreactive residues. Finally, all blocks were dried at 80 °C to remove all solvents.[46]

C. Cell culture

Human SH-SY5Y and HUVEC cell lines were used for axenic and mixed culture in a 3D culture medium (1 × 10^6 cell/ml). These cell lines were cultivated in 75 flaks that contained Dulbecco's Modified Eagle Medium (Gibco, Waltham, MA, USA) (10% fetal bovine serum, 1% penicillin/streptomycin, 1% sodium pyruvate, and 1% L-glutamine) at 95% relative humidity, 5% CO_2, and 37 °C.[47,48]

D. Synthesis of GelMA and construction of 3D co-culture formation

Synthesis of GelMA was carried out according to a previous report.[49] 10 g gelatin (gel, Sigma-Aldrich, St. Louis, MO, USA) was dissolved in 100 ml Dulbecco's phosphate-buffered saline (DPBS, pH = 7.4) at 60 °C until completely dissolved. Then, 8 ml of methacrylic anhydride (MA) was added to the solution at 1 ml per minute while vigorously stirring. After being completely dissolved in 3 h, the solution was diluted to obtain five-fold DPBS to stop the polymerization, and the reaction solution was put in a dialysis membrane to remove unreactive poisonous MA and side products for 1 week. The clean GelMA solution was lyophilized to obtain a porous foam-like structure, and then it was stored at −80 °C under dark conditions.[46]

A 10% wt/wt dried GelMA polymer and 1% wt/wt 2-hydroxy-1-(4-(hydroxyethoxy) phenyl)-2-methyl-1-propanone (Irgacure^{TM} 2959, Ciba Specialty Chemicals, Basel, Switzerland) photo-initiating powder were mixed, and the mixture was dissolved in DPBS to obtain a prepolymer solution. Besides, cell lines and citreohybridonol were suspended in the solution; the prepolymer solution was applied on photomasks, and photo-polymerization was carried out at 6.25 W/cm^2 UV light (360–480 nm) for 50 s (Table I, Fig. 1). Finally, the constructs were washed with DPBS and placed on a six-well plate for 3D cell culture experiments. 3D culture scaffolds were covered with Dulbecco's Modified Eagle Medium (DMEM). The hydrogel-covered 3D cell culture frames were cultivated for 0, 1, 4, 7, and 14 days as axenic without/with citreohybridonol at three different concentrations of 20, 40, and 80 μM.[46,47]

E. Characterization of GelMA

Fourier-transform infrared spectroscopy (FTIR) analysis of freeze-dried hydrogel was recorded via a Thermo Scientific

TABLE I. Parameters of the photo-polymerization process.

Parameter	Value
UV exposed time	50 s
Distance between the UV probe and the apparatus	55 mm
UV power	6.25 W/cm^2
PI concentration	1%
GelMA concentration	10%
Cell concentration	1 × 10^6 cell/ml (50 μl)
Citreohybridonol	20, 40 and 80 μM in DMSO

© Author(s) 2022

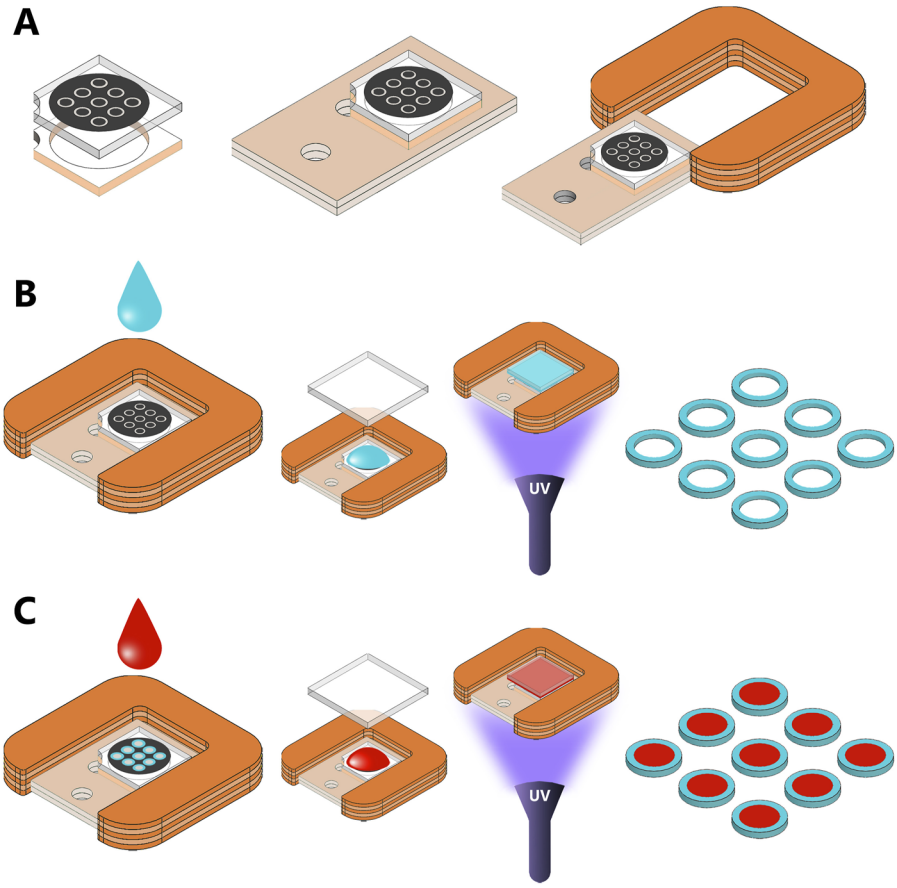


FIG. 1. Schematic representation of the step-by-step fabrication of 3D co-culture scaffolds. (A) The UV mask was mounted onto the frame to be moved into the U-shape apparatus. (B) The cell-laden gel precursor was pipetted onto the glass slide and then sandwiched with another glass slide. The frame was exposed to UV light, and donut-shaped gels were formed. The rest of the precursor solution was washed away. (C) Then, a second droplet of the cell-laden gel precursor solution was pipetted onto the glass slide and sandwiched again with another glass slide. The frame was exposed to UV light again, and disk-shaped gels were formed inside the previously cured donut-shaped gels.

Nicolet^{TM} iS50 FTIR spectrometer (USA) equipped with a diamond ATR (Attenuated Total Reflectance) module and a DTGS (Deuterated-Triglycine Sulfate) detector. The resolution was adjusted to 4 cm^{-1}, and both references and samples were scanned between 4000 and 400 cm^{-1} for 128 cycles. Every sample was tested in triplicate, and the results were analyzed with the built-in software of the FTIR spectroscope.[50] In addition, surface topography of GelMA hydrogels was investigated by Atomic Force Microscopy (AFM) (Easyscan 2, Nanosurf AG, Liestal, Switzerland) via Nanosurf Easyscan 2 software. The scanning procedure was operated in the tapping mode using a silicon cantilever probe Tap190Al-G (Buged Sensors, Sofia, Bulgaria) with the parameters of a force constant of 48 N m^{-1} and a resonance frequency of 65 kHz.

F. Cell viability test

Cell viability was evaluated with the cytotoxic test. The test was carried out using a 3-(4,5-dimethylthiazol-2-yl)-2, 5-diphenyl-tetrazolium bromide (MTT) (Cat No. M-2128, Sigma-Aldrich, St. Louis, MO, USA) assay. 2 ml MTT: DMEM (1:9) solution was added to the 3D culture medium, and the mixture was cultivated for 4 h in a 5% CO_2 humidified incubator at 37 °C. The incubation was stopped by adding 2 ml dimethyl sulfoxide (CAS No. 67-68-5, Merck Millipore, Burlington, MA, United States); the solutions were mixed for 15 minutes at 37 °C, and then the absorbance values were measured at 570 nm.[51]

G. Immunohistochemical staining

The procedure was repeated six times for each concentration and each time step, e.g., six repeats for day 0 and 20 μM concentration and so on. By experimenting four concentrations (control, 20, 40, and 80 μM) at five time intervals (days = 0, 1, 4, 7, and 14), there were 120 cases in total. Well plates for each of these experiments were washed with DPBS and were fixed by 4% paraformaldehyde–PBS mixture for 10 minutes, permeabilized by 0.05% Triton X-100 (Sigma-Aldrich, St. Louis, MO, USA) for 5 minutes and blocked with 1% BSA (Sigma-Aldrich, St. Louis, MO, USA) solution for 1 h for clarifying the background painting. Then, plates were washed with DPBS. The angiopoietin 1 polyclonal antibody (bs-0800R) (Bioss, USA) was used to display HUVEC cells; The Nestin antibody (sc-23927) (Santacruz, USA), formed by diluting 1:800 with 1% BSA-DPBS, was used to display SH-SY5Y cells. After adding the antibodies, the encapsulated cells were incubated overnight at 4 °C. The antibodies were removed, and the plates were washed by DPBS. The goat anti-mouse IgG H+L secondary antibody, FITC (62-6511) (Invitrogen, USA), and Alexa FluorTM

© Author(s) 2022

680 phalloidin (A22286) were used for HUVEC and SH-SY5Y, respectively, as secondary antibodies, and the cells were incubated for 1 h at room temperature. After incubation, the antibodies were removed by DPBS. The cells were incubated with the DAPI antibody (4′, 6-diamidino-2-phenylindole) (Sigma-Aldrich, St. Louis, MO, USA) (1:20; DAPI:1% BSA-DPBS) that was used to detect live and stable cells for 45 min at room temperature. DAPI was removed by DPBS, and the samples were put in Entellan (Sigma-Aldrich, St. Louis, MO, USA) and fixed on the cover slip for monitoring under a confocal microscope (Carl Zeiss AG, Oberkochen, Germany).

H. Statistical analysis

The whole absorbance results were processed via GraphPad Prism 8 software. Two-way analysis of variance (ANOVA) followed by post-hoc Turkey test was considered for statistical analysis of the cytotoxic test results. The level of significance was accepted to be $p > 0.05$.

III. RESULTS

A. GelMA characterization

GelMA synthesis was characterized by comparing FTIR spectra of pure gelatin and GelMA. The key connections in the spectra are indicated (supplementary material Fig. 3). A strong peak at 1650 cm^{-1} indicated amide I primarily. C=O stretching groups and the C–N–H bending bond were detected in the range of 1500–1570 cm^{-1}. The peptide bonds (mainly N–H stretching) were observed in the range of 3200–3400 cm^{-1}. The C–H stretching groups displayed a peak at 3062 cm^{-1}, and gelatin and methacrylate anhydride interaction in GelMA was characterized by a carbon double bond peak at 1640 cm^{-1}.[50] These results indicated that the ideal hydrogel composition was achieved between gelatin and methacrylic anhydride, after which construction of the 3D co-culture formation structure was carried out (Fig. 1).

The morphological features of pure GelMA were investigated via SEM [Figs. 2(a) and 2(b)]. The diameters of gel pores were measured to be 54.92 μm on average. Besides, the roughness of the polymer structure was measured to be 26–30 nm via two- and three-dimensional images from AFM [Figs. 2(c) and 2(d)]. The precision of the alignment and the gel fabrication of the device are the key features in the construction of the 3D cell culture environment. This step was featured by colored and transparent hydrogel posts. 300 μm thick gel posts were fabricated by using square and circle photomask sets. Every unit was individually dyed for observing the alignment and the interfaces of the hydrogel posts (supplementary material Fig. 4). The results proved that there was no gap between hydrogels and masks and cell lines were successfully encapsulated as axenic and mixed with/without citreohybridonol.

B. Cell viability

In this study, HUVECs and SH-SY5Y were cultivated as both axenic and a mixed culture medium to investigate the effects of cell viability and regenerative efficiency of citreohybridonol on damaged brain tissue via a 3D cell microenvironment. First, the effects of the 3D cell culture environment and citreohybridonol on cell viability were tested using the cytotoxic test. All 3D cell culture

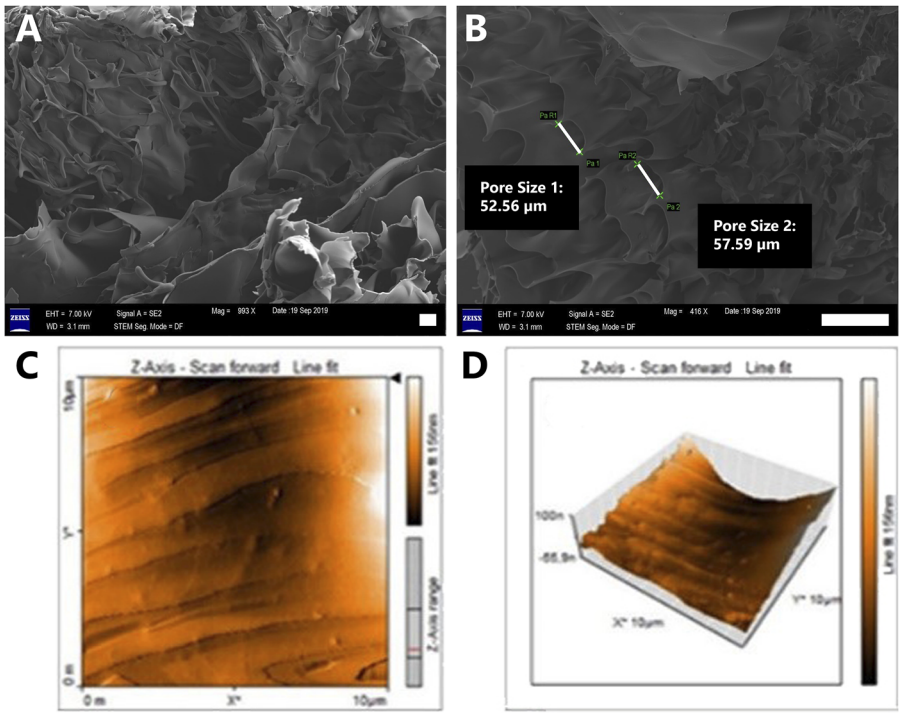


FIG. 2. Scanning electron microscopy (SEM) and topographic images of GelMA. The morphological features of GelMA were investigated by SEM, under (A) 993× magnification and (B) 416× magnification. The diameters of pores were measured to be 54.92 μm. (C) The 2D image from atomic force microscopy (AFM) and (D) the 3D image of AFM analysis. The roughness of the polymer structure was calculated to be 26–30 nm.

© Author(s) 2022

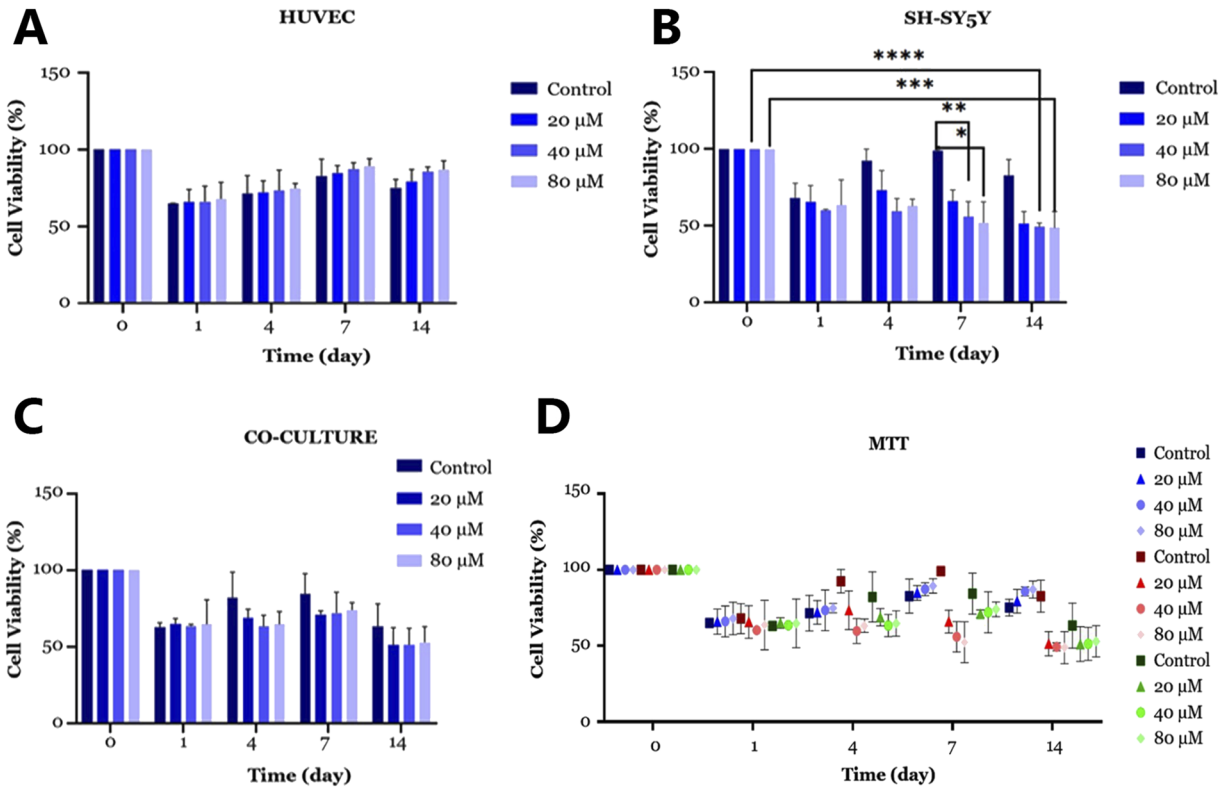


FIG. 3. Histogram of cytotoxic test results. The cell viability increased toward day 7 in the absence of citreohybridonol in (A) HUVECs, (B) SHSY5Y, and (C) mixed co-culture, confirming that the 3D microenvironment was non-toxic for cultural experiments. (D) The entire set of cell viability, with HUVECs shown in blue, SH-SY5Y in red, and co-culture in green. The administration of 40 and 80 μM concentrations of citreohybridonol had a positive effect on HUVECs, which, however, conversely diminished the growth rate of the SHSY5Y cell line on days 7 and 14. (n = 6).

constructions were cultivated for 14 days, and cell viability was controlled on days 0, 1, 4, 7, and 14 (Fig. 3). The cell viability of axenic SH-SY5Y, axenic HUVECs, and mixed culture without metabolites increased toward day 7. These results showed that the 3D microenvironment was non-toxic for cultural experiments. Besides, citreohybridonol showed an inhibitory effect on SH-SY5Y cells based on concentration, whereas it induced the HUVEC cell line in the same period. Thus, these results explained that the increase

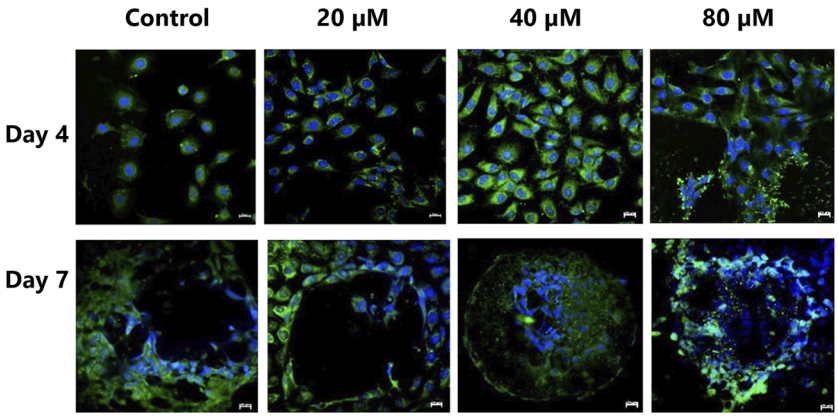


FIG. 4. Immunostaining assay of HUVECs. Exhibition of the positive effects of citreohybridonol in three different concentrations of 20, 40, and 80 μM in comparison with the control group. The top row photos were taken on day 4, and the photos of the bottom row were taken on day 7. All scale bars: 100 μM.

© Author(s) 2022

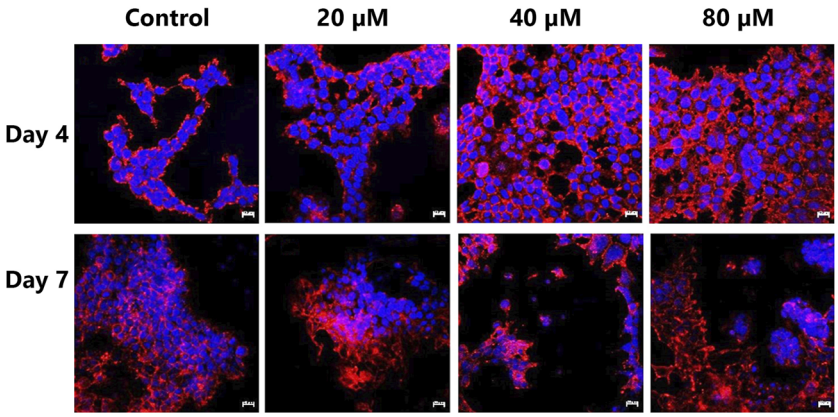


FIG. 5. Immunostaining assay of SH-SY5Y. The assay indicated that the administration of 20, 40, and 80 μM concentrations of citreohybridonol inhibited the cell growth in comparison with the control group. The top row photos were taken on day 4, and the photos of the bottom row were taken on day 7. All scale bars: 100 μM.

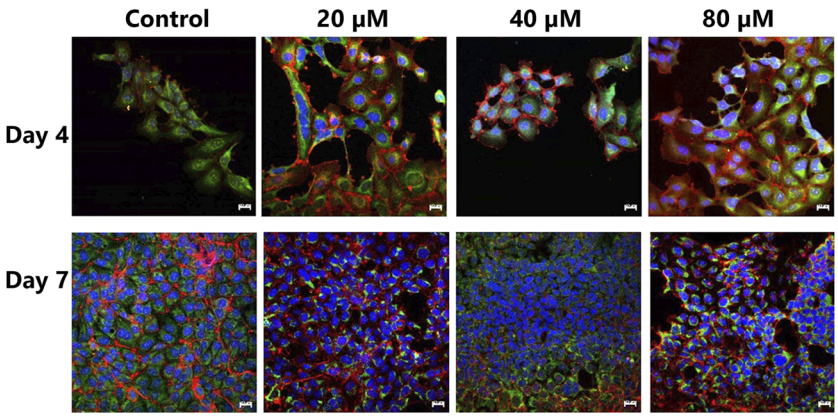


FIG. 6. Co-culture immunostaining assay, indicating that the administration of 20, 40, and 80 μM concentrations of citreohybridonol positively affected and induced the vascularization properties of HUVECss and conversely suppressed the SH-SY5Y cell line, in comparison with the control group. The top row photos were taken on day 4, and the photos of the bottom row were taken on day 7. All scale bars: 100 μM.

in cell viability in the co-culture medium was related to the positive effect of metabolites on HUVECs. The decline in cell viability in GelMA encapsulated axenic SH-SY5Y was proved at 40 and 80 μM metabolite levels on days 7 and 14. On the contrary, the increase in cell viability of encapsulated axenic HUVECs was found at 40 and 80 μM metabolite concentrations on days 7 and 14. The increase in viability in encapsulated co-culture was observed at 40 and 80 μM metabolite levels on days 7 and 14.

C. Immunostaining

The formation of the 3D co-culture microenvironment was visualized by immunostaining, and the mimicking tissues were observed by comparing the DAPI color contrast in all cell types from days 0 to 7. The results proved that the 3D cell culture environment was suitable for the selected cell lines as axenic or mixed culture and overlapped with cell viability analysis. 40 and 80 μM concentrations of citreohybridonol positively affected HUVEC formation on days 4 and 7 (Fig. 4), whereas SH-SY5Y cells, which were visualized in red color, were inhibited in axenic cultures (Fig. 5). 40 and 80 μM concentrations of citreohybridonol suppressed SH-SY5Y cells on days 4 and 7, inducing the vascularization of HUVECs in the mixed 3D cell culture (Fig. 6). Thus, the 3D cell system with citreohybridonol demonstrated its efficiency for potential neuro-regenerative medicine applications.

IV. DISCUSSION

In this study, citreohybridonol, isolated from a sponge-derived fungus *Penicillium atrovenetum*, was selected as a neuro vascularization agent. This compound acts as an anti-neuroinflammatory metabolite in lipopolysaccharide-induced murine microglial cell line BV-2 via variable controlling of the NF-kB and p38 MAPK pathways mediated by the activation of toll-like receptor 4 (TLR-4) signaling under inflammatory conditions. Furthermore, its functional and broadcast effects for the recovery of degenerated neurons have been confirmed in Parkinson's disease (PD), multiple sclerosis (MS), amyotrophic lateral sclerosis (ALS), Alzheimer's disease, stroke, and HIV-associated dementia (HAD).[43,52,53] In order to discuss the comparison of citreohybridonol with previously reported various kinds of neuroprotective, anti-angiogenesis, or angiogenesis compounds from natural sources (terrestrial and marine organisms) and synthetic derives,[54–57] along with Ukgansan (UGS) and Houshiheisan as neurovascular herbal extracts,[58,59] a versatile compound

© Author(s) 2022

that both inhibits the cancer cells and induces blood vein formation was not reported.

Physiological development of native tissues that comprise several cell types and complicated 3D extracellular matrix (ECM) components that contain nutrient transportation systems and cell–cell and cell–microenvironment interactions depends on the position and composition of cells and ECM components.[60,61] 3D tissue engineering methods have overcome 2D culture limitations by tissue construction and cellular complexity replication, providing insights not only about drug screening but also offer time- and cost-efficiency in experiments.[62–67] 3D spatial construction is the major step of microenvironment stability.[46] Previously, we constructed a frame system to build a 3D environment. However, the weld bonding associated with dilation was the main problem.[68] In this study, frames were connected with screws to overcome the dilation, and the fittest 3D structure was achieved. As shown in Fig. 1, the UV mask was first mounted onto the frame in which it was intended to be moved into a U-shaped apparatus. A cell-laden gel precursor was pipetted onto the glass slide. A second glass slide was used to sandwich the precursor droplets. Next, the frame was exposed to UV light followed by washing away the rest of the precursor solution. As a result, donut-shaped gels were formed in this step. In order to cure the gel the second time inside these donut-shaped structures, a second droplet of the cell-laden gel precursor solution was pipetted onto the glass slide, and it was sandwiched again with another glass slide. By exposing the frame to UV light again, disk-shaped gels were formed inside the previously cured donut-shaped gels. 10% GelMA hydrogel was reported as one of the most suitable constructions that mimic the 3D cell culture material in regenerative medicine.

The morphological features of our GelMA, which was investigated with SEM and AFM, showed appropriate porosity (Fig. 2). Its physical features corresponded to material transportation, promoted cell holding, and movement of different cell types in the same area.[68,69] As a result of our cell viability (Fig. 3) and immunostaining assay of HUVECs (Fig. 4), SH-SY5Y (Fig. 5), and co-culture of HUVEC-SH-SY5Y (Fig. 6) presented in this study, the 3D microenvironment, which was constructed via screwed micro-frames and photo-crosslinking of 10% GelMA, was suitable for mimicking the native brain tissue. The histogram of cytotoxic test results that demonstrated an increase toward day 7 in the absence of citreohybridonol in HUVECs, SHSY5Y, and mixed co-culture confirmed that the 3D microenvironment was non-toxic for cultural experiments. The inhibition activity of citreohybridonol on SH-SY5Y cells and then the induction of blood vein formation were demonstrated in this research. Besides, the neurovascular activity of the metabolite was identified via tissue-engineered 3D micro-frame co-culture experiments. These results indicated that citreohybridonol was a unique novel alternative for the treatment of neuroblastoma. This study was also one of the primary research projects that used engineered 3D tissue and natural product chemistry in drug discovery.

On the other hand, citreohybridonol was found as an equilibrium factor between keto-enol tautomers on a five-membered D ring in natural sources.[43,45,70] Tautomer mixtures have been reported in many natural product studies, and tautomerism particularly might have occurred because of the molecular interactions between polar solvents such as CDCl3 and DMSO-d6 and pure compounds.[45] Only one main tautomer can be found dominant under optimal experimental conditions,[71] and only C-17-ketone-tautomer of citreohybridonol was observed via X-ray crystallography analysis without solvents.[49] However, this metabolite was dissolved in DMSO for 3D cell culture experiments in this study and previous studies. The tautomer mixtures will be separated, and the one with an active tautomer or possible synergetic effect will be elucidated in future studies. It can also be discussed that the offered protocol is straightforward and compatible for future studies with different culture environments.

SUPPLEMENTARY MATERIALS

The following are available online: supplementary material Fig. 1: chemical structure of citreohybridonol in DMSO-d6; supplementary material Fig. 2: (a) the drawing structures of stainless-steel solid blocks, (b) frames and photomasks, (c) square photomasks, and (d) circular photomasks; supplementary material Fig. 3: the FTIR spectra of gelatin and GelMA; supplementary material Fig. 4: (a) encapsulation of co-culture by photomasks and (b) hydrogel formation.

ACKNOWLEDGMENTS

S.T. acknowledges the Tubitak 2232 International Fellowship for Outstanding Researchers Award (Grant No. 118C391), the Alexander von Humboldt Research Fellowship for Experienced Researchers, the Marie Skłodowska-Curie Individual Fellowship (Grant No. 101003361), and the Royal Academy Newton-Katip Çelebi Transforming Systems Through Partnership Award (Grant No. 120N019) for financial support of this research. This work was partially supported by the Science Academy's Young Scientist Awards Program (BAGEP), the Outstanding Young Scientists Awards (GEBİP), and the Bilim Kahramanlari Dernegi Young Scientist Award. Opinions, interpretations, conclusions, and recommendations are those of the author and are not necessarily endorsed by the TÜBİTAK.

AUTHOR DECLARATIONS

Conflict of Interest

The authors have no conflicts to disclose.

Author Contributions

Emel Sokullu: Conceptualization (equal); Data curation (equal); Formal analysis (equal); Funding acquisition (equal); Investigation (equal); Project administration (equal). **İrem Polat**: Formal analysis (equal). **Ferhat Can Özkaya**: Formal analysis (equal). **Mona El-Neketi**: Methodology (equal). **Weaam Ebrahim**: Formal analysis (equal). **Misagh Rezapour Sarabi**: Formal analysis (equal); Writing – review & editing (equal). **Gulgun Sengul**: Writing – review & editing (equal). **Savas Tasoglu**: Funding acquisition (equal); Investigation (equal); Methodology (equal); Project administration (equal); Writing – review & editing (equal).

© Author(s) 2022

DATA AVAILABILITY

The data that support the findings of this study are available from the corresponding author upon reasonable request.

REFERENCES

[1] J. M. Maris and K. K. Matthay, "Molecular biology of neuroblastoma," J. Clin. Oncol. **17**, 2264 (1999).
[2] J. R. Park, A. Eggert, and H. Caron, "Neuroblastoma: Biology, prognosis, and treatment," Pediatr. Clin. North Am. **55**, 97–120 (2008).
[3] S. Sajib *et al.*, "Mechanisms of angiogenesis in microbe-regulated inflammatory and neoplastic conditions," Angiogenesis **21**, 1–14 (2018).
[4] B. A. Warren, "Tumor angiogenesis," *Tumor Blood Circulation: Angiogenesis, Vascular Morphology and Blood Flow of Experimental and Human Tumors* (CRC Press, 2020), pp. 49–75.
[5] A. A. Ucuzian *et al.*, "Molecular mediators of angiogenesis," J Burn Care Res. **31**, 158–175 (2010).
[6] S. Qin *et al.*, "Recent advances on anti-angiogenesis receptor tyrosine kinase inhibitors in cancer therapy," J. Hematol. Oncol. **12**, 27 (2019).
[7] K. P. Deshmukh *et al.*, "Recent technological developments in the diagnosis and treatment of cerebral edema," Adv. NanoBiomed Res. **1**, 2100001 (2021).
[8] N. Jiang *et al.*, "Intracranial sensors for continuous monitoring of neurophysiology," Adv. Mater.s Technol. **6**, 2100339 (2021).
[9] A. Birgersdotter, R. Sandberg, and I. Ernberg, "Gene expression perturbation in vitro—A growing case for three-dimensional (3D) culture systems," *Seminars in Cancer Biology* (Elsevier, 2005).
[10] S. Rahmani Dabbagh *et al.*, "3D bioprinted organ-on-chips," Aggregate **00**, e197 (2022).
[11] D. Yigci *et al.*, "3D bioprinted glioma models," Prog. Biomed. Eng. **4**, 113 (2022).
[12] S. Knowlton *et al.*, "Utilizing stem cells for three-dimensional neural tissue engineering," Biomater. Sci. **4**, 768–784 (2016).
[13] A. C. Bilirgen *et al.*, "Plant-based scaffolds in tissue engineering," ACS Biomater. Sci. Eng. **7**, 926–938 (2021).
[14] M. Nooranidoost *et al.*, "A computational study of droplet-based bioprinting: Effects of viscoelasticity," Phys. Fluids **31**, 081901 (2019).
[15] B. Mirani *et al.*, "Microfluidic 3D printing of a photo-cross-linkable bioink using insights from computational modeling," ACS Biomater. Sci. Eng. **7**, 3269 (2021).
[16] M. R. Sarabi *et al.*, "3D printing of microneedle arrays: Challenges towards clinical translation," J. 3D Print. Med. **5**, 65–70 (2021).
[17] M. R. Sarabi *et al.*, "Finger-actuated microneedle array for sampling body fluids," Appl. Sci. **11**, 5329 (2021).
[18] M. Rezapour Sarabi *et al.*, "Biomedical optical fibers," Lab Chip **21**, 627–640 (2021).
[19] S. R. Dabbagh *et al.*, "3D-printed microneedles in biomedical applications," iScience **24**, 102012 (2021).
[20] M. R. Sarabi, A. K. Yetisen, and S. Tasoglu, "Magnetic levitation for space exploration," Trends Biotechnol. **40**, 915 (2022).
[21] M. Rezapour Sarabi, S. A. Nakhjavani, and S. Tasoglu, "3D-Printed microneedles for point-of-care biosensing applications," Micromachines **13**, 1099 (2022).
[22] M. Rezapour Sarabi *et al.*, "Machine learning-enabled prediction of 3D-printed microneedle features," Biosensors **12**, 491 (2022).
[23] X. Fu *et al.*, "Multi-stimuli-responsive polymer particles, films, and hydrogels for drug delivery," Chem **4**, 2084–2107 (2018).
[24] P. Ghasemiyeh and S. Mohammadi-Samani, "Hydrogels as drug delivery systems; pros and cons," Trends Pharm. Sci. **5**, 7–24 (2019).
[25] A. Vedadghavami *et al.*, "Manufacturing of hydrogel biomaterials with controlled mechanical properties for tissue engineering applications," Acta Biomater. **62**, 42–63 (2017).
[26] H. N. Kim and N. Choi, "Consideration of the mechanical properties of hydrogels for brain tissue engineering and brain-on-a-chip," BioChip J. **13**, 8–19 (2019).
[27] M. L. Bedell *et al.*, "Polymeric systems for bioprinting," Chem. Rev. **120**, 10744–10792 (2020).
[28] M. Zhu *et al.*, "Gelatin methacryloyl and its hydrogels with an exceptional degree of controllability and batch-to-batch consistency," Sci. Rep. **9**, 6863 (2019).
[29] E. Sokullu *et al.*, "Microfluidic invasion chemotaxis platform for 3D neurovascular Co-culture," Fluids **7**, 238 (2022).
[30] B. Yenilmez *et al.*, "Development and characterization of a low-cost 3D bioprinter," Bioprinting **13**, e00044 (2019).
[31] M. Ustun *et al.*, "Glioma-on-a-Chip models," Micromachines **12**, 490 (2021).
[32] S. Knowlton *et al.*, "3D-printed microfluidic chips with patterned, cell-laden hydrogel constructs," Biofabrication **8**, 025019 (2016).
[33] E. Lepowsky, M. Muradoglu, and S. Tasoglu, "Towards preserving post-printing cell viability and improving the resolution: Past, present, and future of 3D bioprinting theory," Bioprinting **11**, e00034 (2018).
[34] S. A. Hudu *et al.*, "Cell culture, technology: Enhancing the culture of diagnosing human diseases," J. Clin. Diagn. Res. **10**, DE01 (2016).
[35] D. Antoni *et al.*, "Three-dimensional cell culture: A breakthrough in vivo," Int. J. Mol. Sci. **16**, 5517–5527 (2015).
[36] S. Knowlton and S. Tasoglu, "A bioprinted liver-on-a-chip for drug screening applications," Trends Biotechnol. **34**, 681–682 (2016).
[37] S. Knowlton *et al.*, "Bioprinting for cancer research," Trends Biotechnol. **33**, 504–513 (2015).
[38] S. Tasoglu and U. Demirci, "Bioprinting for stem cell research," Trends Biotechnol. **31**, 10–19 (2013).
[39] S. Knowlton *et al.*, "Bioprinting for neural tissue engineering," Trends Neurosci. **41**, 31–46 (2018).
[40] J. L. von Salm *et al.*, "The status of marine chemical ecology in Antarctica: Form and function of unique high-latitude chemistry," in *Chemical Ecology* (CRC Press, 2018).
[41] M. S. Calabon, R. B. Sadaba, and W. L. Campos, "Fungal diversity of mangrove-associated sponges from New Washington, Aklan, Philippines," Mycology **10**, 6–21 (2019).
[42] K. D. Clevenger *et al.*, "A scalable platform to identify fungal secondary metabolites and their gene clusters," Nat. Chem. Biol. **13**, 895–901 (2017).
[43] K.-H. Cho *et al.*, "Anti-neuroinflammatory effects of citreohybridonol involving TLR4-MyD88-mediated inhibition of NF-$_K$B and MAPK signaling pathways in lipopolysaccharide-stimulated BV2 cells," Neurochem. Int. **95**, 55–62 (2016).
[44] C.-L. Xie *et al.*, "Andrastone A from the deep-sea-derived fungus *Penicillium allii-sativi* acts as an inducer of Caspase and RXR**α**-dependent apoptosis," Fronti Chem. **7**, 692 (2019).
[45] F. C. Özkaya *et al.*, "Isolation and X-ray structure analysis of citreohybridonol from marine-derived *Penicillium atrovenetum*," Nat. Prod. Res. **32**, 840–843 (2018).
[46] U. A. Gurkan *et al.*, "Simple precision creation of digitally specified, spatially heterogeneous, engineered tissue architectures," Adv. Mater. **25**, 1192–1198 (2013).
[47] B. Xiao *et al.*, "Endothelial cell-derived exosomes protect SH-SY5Y nerve cells against ischemia/reperfusion injury," Int. J. Mol. Med. **40**, 1201–1209 (2017).
[48] Y. Zeng and J. Liu, "Role of glypican-1 in endothelial NOS activation under various steady shear stress magnitudes," Exp. Cell Res. **348**, 184–189 (2016).
[49] M. Sun *et al.*, "Synthesis and properties of gelatin methacryloyl (GelMA) hydrogels and their recent applications in load-bearing tissue," Polymers **10**, 1290 (2018).
[50] K. Rahali *et al.*, "Synthesis and characterization of nanofunctionalized gelatin methacrylate hydrogels," Int. J. Mol. Sci. **18**, 2675 (2017).
[51] A. Pouyafar *et al.*, "Treatment of cancer stem cells from human colon adenocarcinoma cell line HT-29 with resveratrol and sulindac induced mesenchymal-endothelial transition rate," Cell Tissue Res. **376**, 377–388 (2019).
[52] N. Aparicio *et al.*, "Role of interleukin 1-beta in the inflammatory response in a fatty acid amide hydrolase-knockout mouse model of Alzheimer's disease," Biochem. Pharmacol. **157**, 202–209 (2018).
[53] S. Schilling *et al.*, "TLR$_2$- and TLR$_3$-activated microglia induce different levels of neuronal network dysfunction in a context-dependent manner," Brain, Behav., Immun. **96**, 80 (2021).

© Author(s) 2022

[54]N. T. Hiep *et al.*, "Isoflavones with neuroprotective activities from fruits of *Cudrania tricuspidata*," Phytochemistry **111**, 141–148 (2015).
[55]B. Nowruzi, G. Sarvari, and S. Blanco, "Applications of cyanobacteria in biomedicine," in *Handbook of Algal Science, Technology and Medicine* (Elsevier, 2020), pp. 441–453.
[56]L. Zhou *et al.*, "Isolation of enantiomeric furolactones and furofurans from Rubus idaeus L. with neuroprotective activities," Phytochemistry **164**, 122–129 (2019).
[57]S.-F. Liu *et al.*, "Alkaloids with neuroprotective effects from the leaves of Isatis indigotica collected in the Anhui Province, China," Phytochemistry **149**, 132–139 (2018).
[58]Y. Kim *et al.*, "Simultaneous determination of the traditional herbal formula Ukgansan and the in vitro antioxidant activity of ferulic acid as an active compound," Molecules **23**, 1659 (2018).
[59]H. Wang *et al.*, "Houshiheisan compound prescription protects neurovascular units after cerebral ischemia," Neural Regener. Res. **9**, 741 (2014).
[60]W. Xiao *et al.*, "Synthesis of photocrosslinkable hydrogels for engineering three-dimensional vascular-like constructs by surface tension-driven assembly," Mater.Sci. Eng.: C **116**, 111143 (2020).
[61]S. Moon *et al.*, "Layer by layer three-dimensional tissue epitaxy by cell-laden hydrogel droplets," Tissue Eng., Part C **16**, 157–166 (2010).
[62]D.-H. Kim *et al.*, "Dissolvable films of silk fibroin for ultrathin conformal bio-integrated electronics," Nat. Maters **9**, 511–517 (2010).
[63]D. Lam *et al.*, "Optimizing cell encapsulation condition in ECM-Collagen I hydrogels to support 3D neuronal cultures," J. Neurosci. Methods **329**, 108460 (2020).
[64]R. Y. Tam, L. J. Smith, and M. S. Shoichet, "Engineering cellular microenvironments with photo-and enzymatically responsive hydrogels: Toward biomimetic 3D cell culture models," Acc. Chem. Res. **50**, 703–713 (2017).
[65]F. Somayeh, "Anti-cancer effect of a new monoorganotin Schiff base complex, [N-(3, 5-Oxidobenzylidene)-4-chlorobenzyhdrazidato](0-methylbenzyl) aquatin (IV) chloride on human breast cancer cells and mammospheres/Somayeh Fani," University of Malaya, 2017.
[66]L. Wang *et al.*, "Bioinspired engineering of organ-on-chip devices," in *Biological and Bio-Inspired Nanomaterials,* edited by S. Perrett, A. Buell, and T. Knowles (Springer, Singapore, 2019), pp. 401–440.
[67]U. A. Gurkan *et al.*, "Emerging technologies for assembly of microscale hydrogels," Adv. Healthcare Mater. **1**, 149–158 (2012).
[68]F. Ersoy and E. Sokullu, "A compartmental 3D scaffold fabrication and alignment device for neurovascular co-culture and tri-culture," Biomed. Phys. Eng. Express **5**, 035034 (2019).
[69]C. H. Lin *et al.*, "Stiffness modification of photopolymerizable gelatin-methacrylate hydrogels influences endothelial differentiation of human mesenchymal stem cells," J. Tissue Eng. Regener. Med. **12**, 2099–2111 (2018).
[70]Z. Cheng *et al.*, "Two new meroterpenoids and two new monoterpenoids from the deep sea-derived fungus *Penicillium* sp. YPGA11," Fitoterapia **133**, 120–124 (2019).
[71]C. A. Slabber, C. D. Grimmer, and R. S. Robinson, "Solution conformations of curcumin in DMSO," J. Nat. Prod. **79**, 2726–2730 (2016).

© Author(s) 2022